

AD-A046 885

ROYAL AIRCRAFT ESTABLISHMENT FARNBOROUGH (ENGLAND)
THE SPECTRAL RESPONSE OF PB/SNTE DETECTORS. (U)

F/G 17/5

UNCLASSIFIED

RAE-TR-77066

DRIC-BR-58456

NL

| OF |
ADA046885

12



END

DATE

FILMED

12-77

DDC

TR 77066

AD A 046885

UNLIMITED

(18) DRIC



ROYAL AIRCRAFT ESTABLISHMENT

(9) *
Technical Report 77066

(11) May 1977

(12) 28p.

(6) THE SPECTRAL RESPONSE OF
Pb/SnTe DETECTORS.

by

(10) B. Ellis

*

DDC
RECEIVED
NOV 22 1977
D

Procurement Executive, Ministry of Defence
Farnborough, Hants

AD No. _____
DDC FILE COPY

310450

JB

ACCESSION for	
NTIS	White Section <input checked="" type="checkbox"/>
DDC	Buff Section <input type="checkbox"/>
UNANNOUNCED	<input type="checkbox"/>
JUSTIFICATION	
BY	
DISTRIBUTION/AVAILABILITY CODES	
Dist.	AVAIL. and/or SPECIAL
A	

UDC 621.384.3 : 546.815'811'24 : 551.521.3

ROYAL AIRCRAFT ESTABLISHMENT ✓

Technical Report 77066 ✓

Received for printing 11 May 1977

THE SPECTRAL RESPONSE OF Pb/SnTe DETECTORS

by

B. Ellis

SUMMARY

The effect of the Burstein-Moss shift of the absorption edge on the spectral response of Pb/SnTe detectors is calculated. Calculated spectral responses are compared to published curves for a number of detectors (both homostructure and heterostructure) and some inferences concerning the surface recombination rates and diffusion lengths are drawn. The figure of merit M^* is evaluated for a range of detectors with different cut-off wavelengths.

Departmental Reference: Space 526

Copyright
©
Controller HMSO London
1977

DDC
RECEIVED
NOV 22 1977
D

310 450

JB

LIST OF CONTENTS

	<u>Page</u>
1 INTRODUCTION	3
2 DETAILS OF THE CALCULATIONS	3
3 THE EXPERIMENTAL DATA USED	5
4 RESULTS	6
4.1 Burstein-Moss shift of the absorption edge	6
4.2 Effect of the Burstein-Moss shift on spectral response	7
4.3 Spectral response of heterostructure detectors	8
4.4 M^* calculations	10
5 CONCLUSIONS	12
Acknowledgments	13
References	14
Illustrations	Figures 1-11
Report documentation page	inside back cover

1 INTRODUCTION

For detection in the important 8-14 μ m atmospheric window the alloy system Pb/SnTe shows considerable promise¹ and detectors with background limited performance at 77 K have been made^{2,3}. Since it is difficult to produce low carrier concentration material in the Pb/SnTe system, due to the relatively large deviations from stoichiometry that it can accommodate, virtually all devices are designed to work in the photovoltaic mode (throughout this paper the term 'doping level' will be taken to include deviations from stoichiometry). A p-n junction, Schottky barrier or a Pb/SnTe-PbTe heterojunction is used to provide the necessary potential barrier. In order to achieve low reverse saturation currents (j_0), and thus high zero-bias impedance (implying high responsivity and detectivity), it is desirable to fabricate junction detectors with relatively high doping levels on each side of the junction. However, associated with the narrow energy gap of these materials, essential to achieve the desired spectral response, are extremely low values of effective mass. Consequently, the density of states is low and the Burstein-Moss shift of optical energy gap due to band filling can be very large indeed. Due to the location of the energy band extrema near the L point (ie, away from the zone centre) in the Pb/SnTe alloys the valence band is virtually a mirror image of the conduction band and large Burstein-Moss shifts are found in p-type as well as in n-type samples. In a p-n junction detector it is thus possible to find different shifts in the p and n regions. As the tin content of the alloy is increased to give smaller energy gaps, so the effective masses get smaller and the Burstein-Moss shift, for a given carrier concentration, becomes still larger. Thus, only to a limited extent can the shift of absorption edge, and the consequent shift in the spectral response of Pb/SnTe detectors, be offset by the choice of an alloy composition with a smaller energy gap. The present work describes calculations of the magnitude of the Burstein-Moss shift and its effect upon the spectral response of Pb/SnTe detectors for a range of alloy compositions spanning the 8-14 μ m region of the spectrum. A preliminary report of this work has been presented earlier⁴ but the calculations have now been extended to include an evaluation of the M^* figure of merit, appropriate for thermal imaging applications and to cover the spectral response of heterojunction detectors.

2 DETAILS OF THE CALCULATIONS

It was assumed that the junction, either a p-n junction in Pb/SnTe or an n-type PbTe/p-type PbSnTe heterojunction, was formed by an abrupt interface between two regions. An n on p structure is assumed throughout and all the

results apply to 77 K. No account was taken of possible gradations in carrier concentration and the depletion region was assumed to be narrow compared to the carrier diffusion lengths. In the case of the heterostructure any restriction of the current flow due to possible 'notches' in the band structure were also ignored, as were gradations in the alloy composition. However, the calculations were extended to include the case of a surface layer consisting not of PbTe but of a Pb/SnTe alloy of low tin content.

With these assumptions the short circuit photocurrent J_{sc} and the reverse saturation current j_0 were calculated (equations (6-34) and (6-35) of Ref 1) from the minority carrier diffusion relations. In calculating the detectivity it was assumed that the detector was Johnson noise limited and the noise voltage was calculated from j_0 . Only the case of zero bias was considered.

In all the calculations the absorption coefficients used were modified from those appropriate to carrier-free material by the calculated Burstein-Moss shift. A simplification introduced in this calculation was the assumption that the constant energy surfaces were spherical rather than ellipsoidal but, since the density of states effective mass used was that calculated from the known values for ellipsoidal surfaces, this is not likely to have affected the results seriously. This simplification was necessitated by the absence of any theoretical results for the Burstein-Moss shift in materials in which both bands have ellipsoidal energy surfaces.

A range of alloy compositions was considered, all with energy gaps in the 8-14 μ m region of the spectrum and for each alloy composition the calculations were performed for several different carrier concentrations (in the range $5 \times 10^{16} \text{ cm}^{-3}$ to $1 \times 10^{18} \text{ cm}^{-3}$). Due allowance was made for the variation of carrier transport parameters with carrier concentration. For each case the surface layer and bulk photocurrents, giving the detectivity, were computed for a range of surface layer thicknesses (t) so that the optimum thickness could be found. This was done for various surface recombination rates although the values of $s = 0$ and $s = 10^6 \text{ cm s}^{-1}$ were mostly used.

Since an idealised junction is assumed the values of detectivity obtained are very high, about an order of magnitude greater than those obtained in practice. However, this is of little consequence since the conclusions in this paper rely on comparative rather than absolute values of detectivity. For this reason no account has been taken of the background limit to detector performance.

In addition to the tabulation of detectivities as a function of wavelength the computation included an evaluation of the figure-of-merit M^* for each set

of detector parameters. This quantity is defined by the relation⁵

$$M^*(\lambda_c, R, T_0) = \int_0^{\lambda_c} D^*(\lambda) \tau(\lambda) \left(\frac{W}{T} \right)_{T_0} d\lambda$$

where $D^*(\lambda)$ is the spectral detectivity of a detector with a long wavelength cut-off λ_c viewing a black body source of spectral radiant emittance W at temperature T_0 and distance R . The transmission of the atmosphere between source and detector is $\tau(\lambda)$. Throughout the present calculations T_0 was taken to be 295 K.

3 THE EXPERIMENTAL DATA USED

Many of the parameters required for these calculations vary with alloy composition and while a considerable volume of experimental data on Pb/SnTe is now available it is far from complete. Reliable absorption data for 77 K is sparse, even for the parent lead salt compounds. In addition, since samples with low carrier concentrations have only recently become available most published absorption coefficient data shows evidence of the Burstein-Moss shift and only rarely have measurements been extended to sufficiently high photon energies to give points unaffected by such shifts. The procedure adopted in the present work was to seek 77 K data which extended to sufficiently high energies for the theoretical relation $K = A(h\nu - E_G)^{\frac{1}{2}}$ for direct transitions to be applicable. The constant A was then derived from the high energy data and the theoretical relation was used to generate the carrier-free absorption curves at lower photon energies.

The only absorption data for the Pb/SnTe alloys which extends to sufficiently high values is that of Tao and Wang⁶, obtained at 81 K for 20% SnTe alloys (ie, $x = 0.2$). This gives $A = 1.78 \times 10^4 \text{ cm}^{-1} \text{ eV}^{-\frac{1}{2}}$ and this value was used for all alloy compositions except the low tin content alloy considered as the surface layer of a heterostructure device. For PbTe itself the situation is less satisfactory; the only absorption data for high photon energies is that of Scanlon⁷ but this was obtained at 300 K. In the absence of other data and any indication of the way in which A varies with temperature in PbTe the value of A ($3.18 \times 10^4 \text{ cm}^{-1} \text{ eV}^{-\frac{1}{2}}$) derived from this data has been used in the present work for the heterostructure calculations. It should be noted that the conclusions are not critically dependent upon the value assigned to A .

Measurements of carrier mobilities at 77 K have been reported by a number of workers⁸⁻¹¹ and, although these show some spread due to differences in material quality, the variation of mobility with carrier concentration may be clearly identified. Over the range of alloy compositions considered (the low Sn content alloys excepted) the variation of mobility with SnTe content is smaller than the spread of the available data and has been ignored. In selecting mobility data, in order to obtain the carrier diffusion constants and diffusion lengths, preference was given to the highest reported values for a given carrier concentration. The carrier life-time at 77 K has only been measured by two groups of workers^{12,13} both of whom used photoconductive techniques and reported values $\sim 1.5 \times 10^{-8}$ s for carrier concentrations and alloy compositions in the range of interest here. The dominant recombination mechanism has not been established. In the absence of other information, therefore, the above value has been assumed throughout the present calculations. It should be noted that the resulting carrier diffusion lengths are quite long (up to 25 μm) and a moderate degradation in carrier life-time is unlikely to have a serious effect on the predicted performance.

Measurements of the carrier effective masses over a range of alloy compositions have been made by Butler¹² (magneto-emission) and at 18% SnTe by Ellis and Moss¹³ (cyclotron resonance). Assuming the conduction and valence bands to be mirror images and taking the longitudinal to transverse mass ratio to be 10.5 at 4.2 K, the transverse effective masses as a function of alloy composition may be obtained from Butler's data. The agreement with the cyclotron resonance data for 18% SnTe is excellent. These results were transformed to give 77 K values using the ratio obtained for 18% material by Ellis and Moss¹⁴ whose value of 7.7 for the effective mass anisotropy was used at that temperature.

4 RESULTS

4.1 Burstein-Moss shift of the absorption edge

Fig 1 shows the calculated absorption constant in a Pb/SnTe alloy with an energy gap of 0.08 eV (15.5 μm). The effect of introducing even a relatively small concentration of free carriers, $5 \times 10^{17} \text{ cm}^{-3}$, is most marked. For a detector with an optimised surface layer thickness t (generally 0.1-0.2 L_p , where L_p is the minority hole diffusion length) and for carrier diffusion lengths of $\sim 20 \mu\text{m}$ the absorption constant should be at least 800 cm^{-1} , giving $Kl \sim 2$ in 24 μm . It will be seen from the curves of Fig 1 that for a carrier concentration, N , of $5 \times 10^{17} \text{ cm}^{-3}$ this condition is not met for wavelengths longer than $\sim 10.5 \mu\text{m}$, while if $N = 10^{18} \text{ cm}^{-3}$ it is 8.4 μm before adequate absorption occurs. Thus, bearing in mind that carrier concentrations of this

magnitude are indeed employed in the fabrication of Pb/SnTe detectors, it is evident that the likely effect on detector performance is large.

4.2 Effect of the Burstein-Moss shift on spectral response

If the surface recombination velocity is low ($s \sim 0$) it is found that the surface layer thickness for highest detectivity⁴, for given carrier concentrations, is $\sim 0.1 L_p$. Fig 2 shows how, for detectors optimised in this way, the spectral response for $x = 0.25$ is changed as the carrier concentration levels are increased (only junctions with equal doping levels are considered in this section). It is evident that at levels up to $1 \times 10^{17} \text{ cm}^{-3}$ the Burstein-Moss shift has little effect upon the shape of the spectral response. However, as the doping is increased to $5 \times 10^{17} \text{ cm}^{-3}$ the peak response shifts from $13 \mu\text{m}$ to $7.5 \mu\text{m}$. For $1 \times 10^{18} \text{ cm}^{-3}$ the effect is still more pronounced. Although higher peak detectivity is obtained with the higher carrier concentrations the long wavelength response of such detectors is severely curtailed (by a factor of 4 at $14 \mu\text{m}$ for $N = 1 \times 10^{18} \text{ cm}^{-3}$). The marked changes in spectral response that occur as the doping level changes imply that if a given spectral response is desired (eg, in an array) tight control over the carrier concentrations must be exercised.

Spectral responses calculated for the case of high surface recombination velocities (Fig 3) are similar in shape to those for the case of negligible surface recombination apart from the steeper fall-off of the response towards shorter wavelengths. The principal effect of high surface recombination rates is a reduction in detectivity by a factor of ~ 2 . This is a consequence of the increase in j_0 which occurs for high values of s .

Many published spectral response curves, particularly those for earlier detectors, are sharply peaked with a steep fall-off at short wavelengths. Frequently this has been attributed simply to high surface recombination rates. Thus it is of interest to attempt to fit calculated response curves to those published. Fig 4 shows the results of such a procedure for the Plessey detector² 94/13. Both the measured response and the calculated curve have been normalised (the calculated value is higher than the experimental result by about a factor of 10). It is evident that an extremely close fit is obtained with carrier concentrations ($4 \times 10^{17} \text{ cm}^{-3}$), close to those used in practice. The choice of carrier concentration is quite critical if a good fit to the shape of the response on the long wavelength side of the peak is to be obtained. This is due to the influence of the Burstein-Moss shift. Further, a high value of surface recombination velocity is indeed required. However, this, on its own,

is not sufficient to give the extremely steep fall-off in performance at shorter wavelengths. In order to produce this it is necessary to assume that the surface layer thickness is of the order of a minority hole diffusion length ($t/L_p \sim 0.8$ where $L_p = 21.9 \mu\text{m}$). This of course, is far from optimum and dramatically reduces the collection efficiency for photo-carriers produced in the surface region by short wavelength radiation. The implication is that the junction in this detector was far too deep. The alternative possibility, that of poor diffusion length in a thinner surface layer does not yield such a steep fall-off. An adequate thickness for absorption of short wavelength light (producing photo-carriers subsequently lost to the surface) must be provided. A further noteworthy feature is that in order to make the peak wavelengths of the responses coincide (at $10.4 \mu\text{m}$), it was necessary to assume that the alloy had an energy gap corresponding to $12.5 \mu\text{m}$; this provides a further illustration of the effect of the Burstein-Moss shift. Somewhat similar considerations apply to the heterojunction responses considered in section 4.3.

4.3 Spectral response of heterostructure detectors

Recently heterostructures have been used for the detection of 8-14 μm radiation³. One of the attractive features of a structure in which a surface layer of PbTe is used is that the long wavelength absorption (ie, for wavelengths beyond the absorption edge of PbTe) occurs in the bulk Pb/SnTe material on the side of the junction remote from the surface of the detector. As far as carriers generated by long wavelength radiation are concerned, therefore, there are no losses due to surface recombination. An additional advantage is the use of a higher energy gap material on one side of the junction which leads to lower values of j_0 and hence to higher values of zero bias impedance.

The published spectral responses of heterostructure devices do indeed show a long wavelength response which falls off relatively slowly towards shorter wavelengths. The average slope of the Santa Barbara detector response³, for example, is nearly ideal (ie, unity) in the region 6-10 μm (Fig 5). However, for wavelengths at which the incident radiation is strongly absorbed in the PbTe surface layer the response of this detector is far lower, as shown by the sharp drop in response for wavelengths below 6 μm .

As may be seen from the normalised spectral responses shown in Fig 5, most of the important features of the spectral response of this detector (No. 19-3) measured at 82 K) may be accounted for by the simple abrupt junction heterostructure model used in the present calculations. In particular the sharp drop in response at wavelengths shorter than 6 μm is well reproduced provided

that a high surface recombination rate $s = 10^7 \text{ cm s}^{-1}$ is used and the surface layer thickness $t = 0.3 L_p$ (ie, $7.4 \mu\text{m}$) is rather greater than that which gives optimum performance when $s = 0$. It was necessary to assume that the surface PbTe layer contained a small amount of SnTe ($x \sim 0.015$) in order to give the drop in performance at the observed wavelength. Since the growth was by liquid phase epitaxy this is not unreasonable.

Relatively low carrier concentrations were assumed in the calculations ($p = 1 \times 10^{17} \text{ cm}^{-3}$, $n = 4 \times 10^{16} \text{ cm}^{-3}$) and consequently the Burstein-Moss shifts are negligible, thus giving the observed sharp long wavelength cut-off ($p = 5 \times 10^{17} \text{ cm}^{-3}$ gives a peak strongly displaced to shorter wavelengths cf Fig 2). Two aspects of the observed response are not reproduced in the calculated curves. These are the slightly lower ($\sim 15\%$) performance observed in the $6\text{-}10\mu\text{m}$ region and the rather higher detectivity observed at short wavelengths ($3\text{-}4.5 \mu\text{m}$). It must be concluded that the explanation of these features would require further refinement of the model; however, it is of interest to note that both of these features change markedly³ when the detector is cooled to 60 K.

The calculated peak detectivity (ignoring background photon noise) for the Santa Barbara detector is $8.3 \times 10^{11} \text{ cm W}^{-1} \text{ Hz}^{\frac{1}{2}}$ and is an order of magnitude greater than that observed. Much of the discrepancy is the result of the poorer junction quality obtained in practice ($R_0 A = 2.64 \Omega \text{ cm}^2$ compared with the calculated value of $64.6 \Omega \text{ cm}^2$; D_{pk}^* varies approximately as $\sqrt{R_0}$).

Another heterostructure detector response which exhibits a sharp drop in detectivity at shorter wavelengths is that of the Plessey device HGF 4/1. As is evident from Fig 6, this too is well fitted by a curve calculated with the assumption of a high surface recombination rate ($s = 10^7 \text{ cm s}^{-1}$). Again, relatively low carrier concentrations are needed in order to give the sharp long wavelength cut-off. However, in order to provide a close fit to the short wavelength part of the response it is necessary to assume that the lifetime in the surface layer is shorter than the assumed bulk value (by a factor of about 25, giving $\tau \sim 0.6 \text{ ns}$) so that the diffusion length is reduced to $4.96 \mu\text{m}$. Further, a surface layer thickness equal to this diffusion length is required, ie, $t/L_p = 1.0$. These parameters were derived from a large number of trial fittings. The high value of t/L_p means that a high proportion of the photo-carriers produced in the surface region diffuse to the surface rather than to the junction and thus do not contribute to the photocurrent. The surface layer thickness governs the extent to which short wavelength radiation (ie, that below the cut-off wavelength

of the surface layer material) is absorbed in the surface layer or is transmitted through the junction to the bulk Pb/SnTe. The choice of t thus strongly affects the shape of the calculated short wavelength response.

It may be seen that only relatively minor features of the spectral response (such as the subsidiary peak at $\sim 5.6 \mu\text{m}$) are not accounted for by the calculated curve. While these details may require a more sophisticated model it is important to emphasise that the essential features of the response are obtained from a relatively simple model. Moreover, in the case of the Plessey detector, as for the Santa Barbara detector, the simple model demonstrates that attention must be paid both to the reduction of surface recombination rates and to the correct choice of surface layer thickness if good short wavelength responses are to be obtained.

Precise fitting of the short wavelength tail required the assumption that the surface layer was a low tin content Pb/SnTe alloy ($x = 0.066$). This is consistent with the method of production of the device. The calculated peak D^* is 7.8×10^{11} and again this shows the scope for improvement, through better junction quality, in heterostructure devices.

4.4 M^* calculations

For devices which are to be used to detect radiation which has been propagated through a long atmospheric path, thermal imaging devices for example, the optimum design of detector is influenced by the transmission characteristics of the atmospheric path. In order to assess this effect the detectivity values calculated for Pb/SnTe detectors were used to calculate the figure of merit M^* (defined in section 2) for various atmospheric path lengths, 0, 2, 5 and 10 km*. In all cases the humidity was taken to be 1.0 pre cm/km.

As noted earlier the values of detectivity obtained from these calculations are far higher than those obtained in practice since the junctions have been assumed to be ideal; also the background limit has been ignored. Thus the absolute values of M^* obtained are also high and represent what could be achieved with ideal Pb/SnTe junctions using a very narrow field of view. However, the relative values of M^* are directly applicable to present experience and lead to some conclusions of interest.

Fig 7 shows how M^* varies as a function of the cut-off wavelength (ie, energy gap), for a homojunction detector with equal p and n carrier concentrations of $5 \times 10^{17} \text{ cm}^{-3}$ and for negligible surface recombination.

* The atmospheric transmission data as a function of wavelength was kindly supplied by Mr J. Owen of RSRE (Malvern).

Since the detectivity calculations were carried out for 10 values of surface layer thickness for each set of detector parameters, M^* was computed for each of these cases. Thus for any given set of values of n, p, x and s ten values of M^* were obtained. In order to plot Fig 7 the largest of these M^* values was selected in each case and this means that t/L_p does not have the same value for all the points on a given curve. This variation, examples of which are shown in Fig 8 for two different cut-off wavelengths, was particularly noticeable for the data for long ranges and for high surface recombination rates. It reflects the change in shape and magnitude of the $D^* \nu \lambda$ curves at t/L_p is varied. For the 5km range the change in M^* as t/L_p varies from 0.1 to 1.0 is $\sim 30\%$.

For zero range the curve shown in Fig 7 rises monotonically towards the shorter cut-off wavelengths. At first sight this is somewhat surprising since the black-body source has its emission peak close to $10 \mu\text{m}$. The steady increase in M^* is the result of the higher values of detectivity that are obtained for detectors with relatively short cut-off wavelengths. This in turn reflects the higher zero bias impedances which are possible with the higher energy gap material.

Only when the atmospheric transmission is included do the M^* curves exhibit peaks. For all the ranges considered these peaks occur in the vicinity of $9.5 \mu\text{m}$. Thus although the atmosphere is relatively transparent over the $8\text{-}14\mu\text{m}$ band the optimum alloy composition for Pb/SnTe photovoltaic detectors gives a cut-off wavelength at the short wavelength end of the band. This is also a consequence of the better junction quality obtainable with higher energy gap materials. For the conditions considered this is as true for 10km ranges as it is for 2 km. Very similar curves are obtained for $s = 10^6 \text{ cm s}^{-1}$ but the values of M^* are lower by a factor of about 2 (Fig 9).

For higher carrier concentrations ($n = p = 10^{18} \text{ cm}^{-3}$) the zero range M^* values are far higher than those for $n = p = 5 \times 10^{17} \text{ cm}^{-3}$, indicating that the effects of the Burstein-Moss shifts of the absorption edge and detectivity peaks are more than offset by the higher values of D^* . For finite atmospheric path lengths the curves obtained for $s = 0$ and $n = p = 10^{18} \text{ cm}^{-3}$ differ quite significantly from those for the lower carrier concentrations (Fig 10). The variation of M^* over the $8.5\text{-}14.5\mu\text{m}$ range is smaller and the short wavelength peak is less marked. This is a result of the broader spectral responses brought about by the Burstein-Moss shift (cf Fig 2). Further the peak values of M^* obtained are very little greater than those for the lower carrier concentrations. Thus the use of carrier concentrations greater than $5 \times 10^{17} \text{ cm}^{-3}$ confers little

advantage for detectors used in systems which entail significant atmospheric transmission. For $s = 10^6 \text{ cm s}^{-1}$ the curves for higher carrier concentration devices (Fig 11) show peaks and are quite similar to those for $5 \times 10^{17} \text{ cm}^{-3}$; again the values of M^* are very little higher than for the $5 \times 10^{17} \text{ cm}^{-3}$ case.

It is evident from Fig 6 that in certain circumstances a relatively small change in alloy composition could in principle lead to large changes in the performance of the detector at long ranges. A shift of $1 \mu\text{m}$ in peak response could change M^* by up to 30%. Fortunately, the composition of Pb/SnTe alloys is generally easily controlled (peak response to better than $0.1 \mu\text{m}$) so that this effect should not be troublesome in practice.

5 CONCLUSIONS

The spectral response of Pb/SnTe detectors may be markedly affected by the Burstein-Moss shift of the absorption edge in the material. For single element detectors designed for such applications as spectroscopic studies this effect is significant, especially at wavelengths close to the long wavelength cut-off of the response. It is also found that for detectors designed for systems involving long atmospheric transmission paths the changes in response due to the Burstein-Moss effect make it pointless to use carrier concentrations above $5 \times 10^{17} \text{ cm}^{-3}$.

All the published spectral responses to which computed curves were fitted showed responses which dropped rapidly with decreasing wavelength. As expected this could be interpreted as evidence of fast surface recombination. However, in order to provide a close fit to some published responses it was necessary to assume that the surface layer thickness as a fraction of the minority carrier diffusion length was far from optimum. In the case of a homojunction detector it was inferred that the diffusion length was satisfactory but that junction was far too deep while for a heterojunction detector it was found that the diffusion length was seriously reduced from the value appropriate to the carrier concentration concerned, most probably due to poor carrier lifetime. For applications for which a good short wavelength response is required attention must therefore be paid to surface quality and to the carrier lifetime in the surface layer.

Within the validity of the assumptions made it was found that detectors used in atmospheric transmission systems should have a peak response at the short wavelength end of the $8\text{-}14\mu\text{m}$ band. For the practical case of devices with high surface recombination velocities the optimum detector has a peak response at $9.5 \mu\text{m}$ for all the ranges considered.

Good fits to published response curves were obtained with a relatively simple abrupt junction model, using practical values of material parameters. However, the available data for the Pb/SnTe alloy system is far from complete and considerable scope remains for studies of the material's electronic properties. The calculations show that if junction quality can be improved the detectivity could rise by at least an order of magnitude before becoming limited by material parameters.

Acknowledgments

The assistance of Mr T.D.F. Hawkins with the computing is gratefully acknowledged.

REFERENCES

<u>No.</u>	<u>Author</u>	<u>Title, etc</u>
1	T.S. Moss G.J. Burrell B. Ellis	Semiconductor Optoelectronics. Butterworths (1973)
2	W. Rolls D.V. Eddolls	Infrared Physics, <u>13</u> , 143 (1973)
3	P.S. Chia J.R. Balon A.H. Lockwood D.M. Randall E.J. Renda L.H. DeVaux H. Kimura	Infrared Physics, <u>15</u> , 279 (1975)
4	B. Ellis	Proceeding of International Conference on semiconductors and semimetals, Nice. (Unpublished) (1973)
5	J.W. Sabey	Proc. IEE. Int. Conf. on low light and thermal systems, p 217 (1975)
6	T.F. Tao C.C. Wang	UCLA Report ENG-7169 (1971)
7	W.W. Scanlon	J. Phys. Chem. Sol., <u>8</u> , 423 (1959)
8	A.R. Calawa T.C. Harman M. Finn P. Youtz	Trans. Met. Soc. AIME, <u>242</u> , 374 (1968)
9	G. Dionne J.C. Woolley	J. Electrochem. Soc., <u>119</u> , 784 (1972)
10	C.R. Hewes M.S. Adler S.D. Senturia	J. Appl. Phys., <u>44</u> , 1327 (1973)
11	I. Melngailis T.C. Harman	Semiconductors and Semimetals. Academic, New York, <u>5</u> , 111 (1970)
12	J.F. Butler	Sol. Stat. Comm., <u>7</u> , 909 (1969)
13	B. Ellis T.S. Moss	Phys. Status Solidi, <u>41</u> , 531 (1970)

REFERENCES (concluded)

<u>No.</u>	<u>Author</u>	<u>Title, etc</u>
14	B. Ellis	Proc. 3rd Photoconductivity Conf.
	T.S. Moss	(J. Phys. Chem. Sol. Suppl.), p 211 (1969)

Fig 1

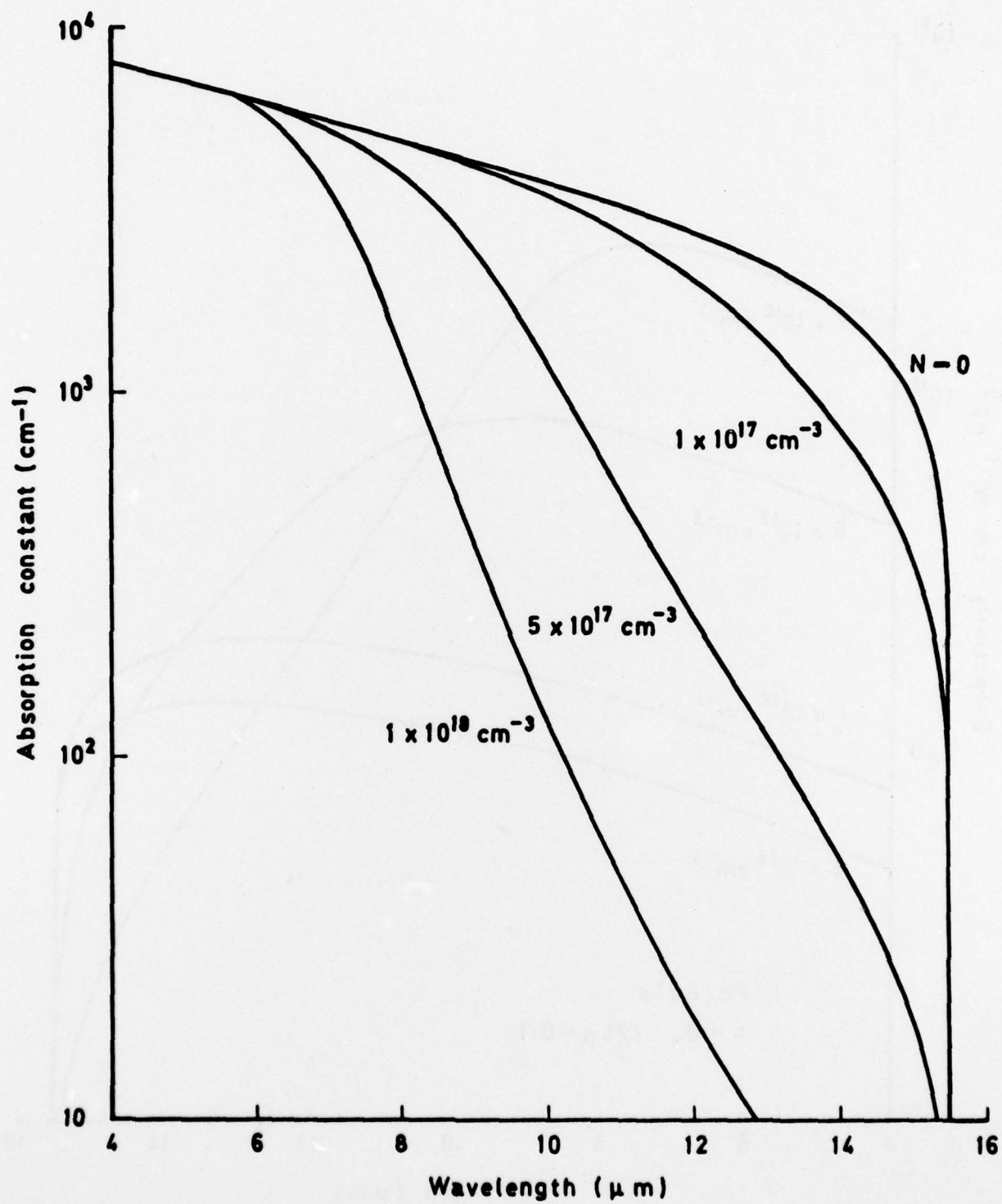


Fig 1 Calculated Burstein-Moss shift of absorption edge in Pb/SnTe at 77 K

Fig 2

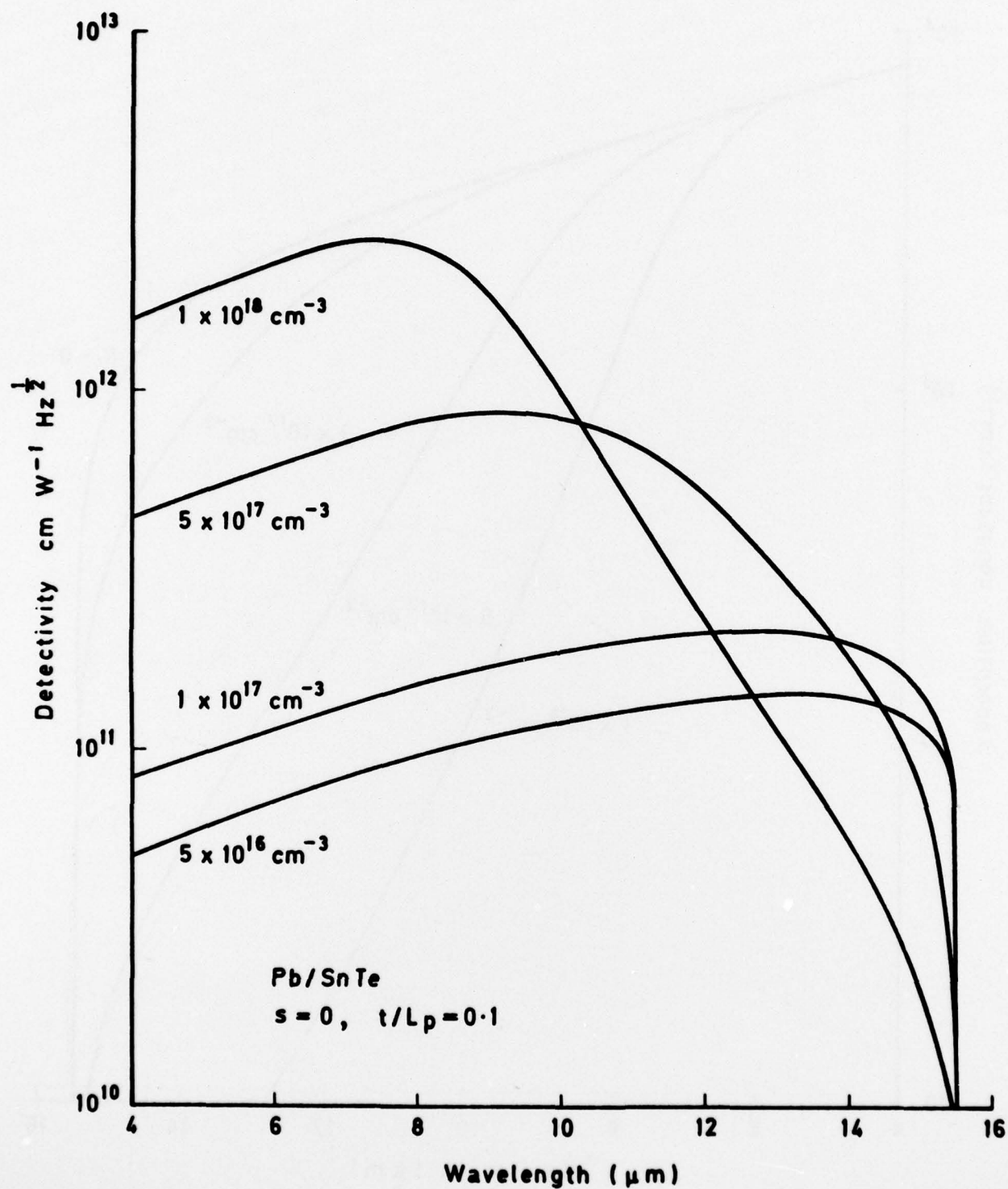


Fig 2 Effect of Burstein-Moss shift on spectral response

Fig 3

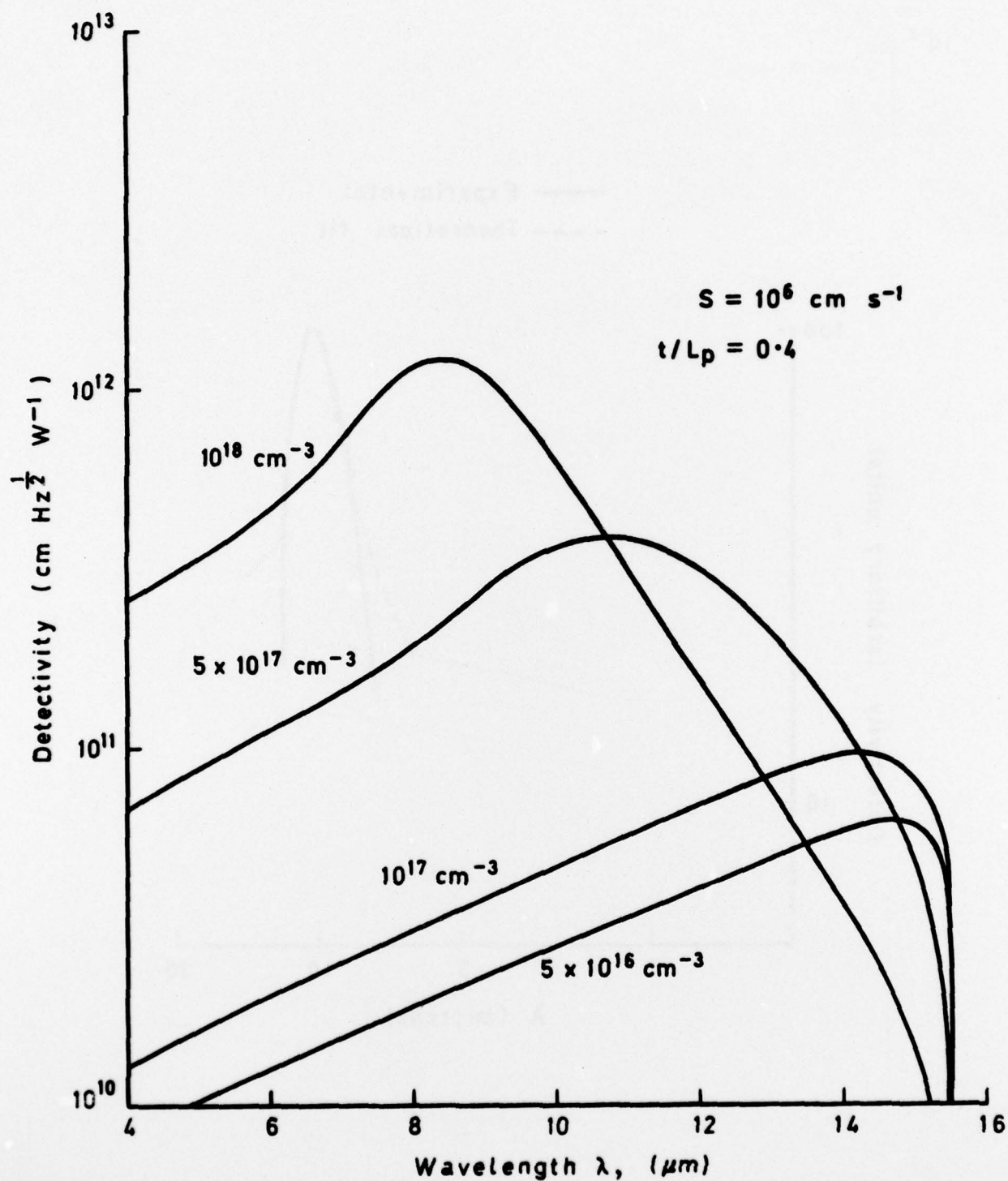


Fig 3 Spectral response of Pb/SnTe detectors with fast surface recombination (carrier concentrations as shown)

Fig 4

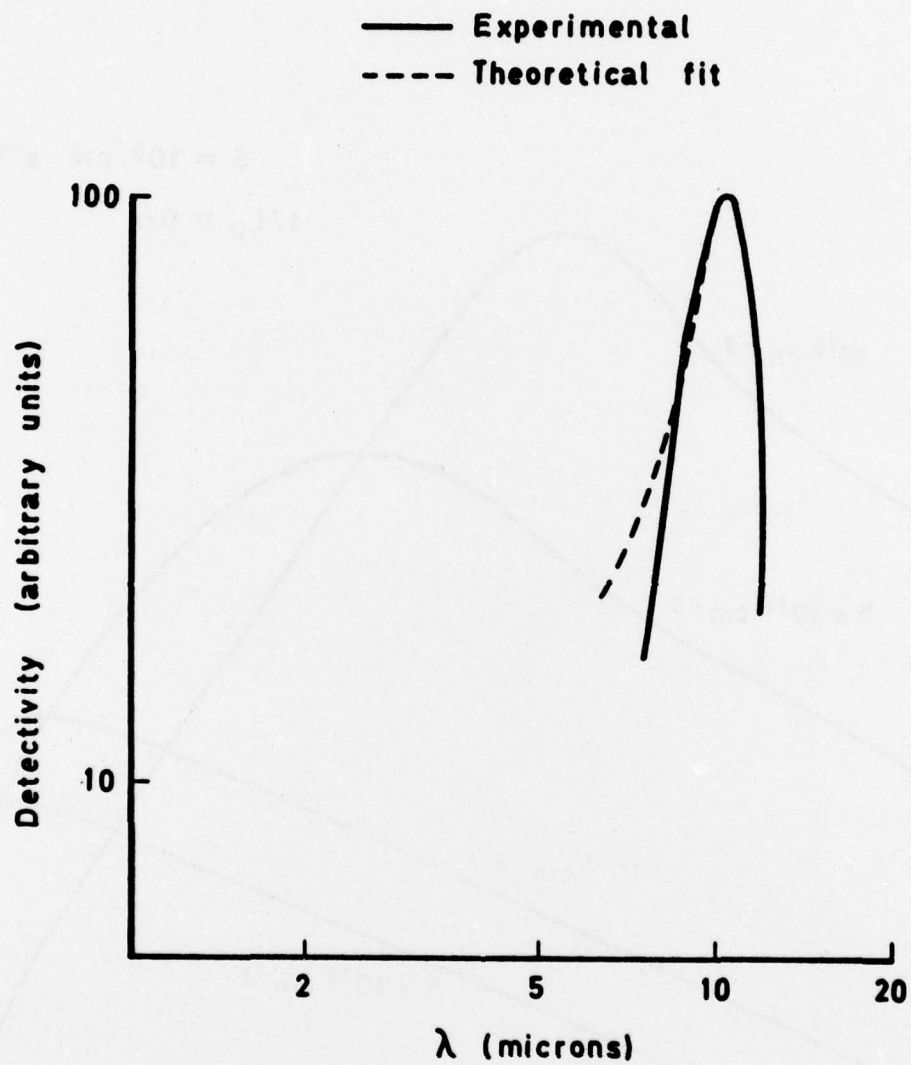


Fig 4 Theoretical fit to response of Plessey detector 94/13
(beyond 9.6 μm the curves coincide)

Fig 5

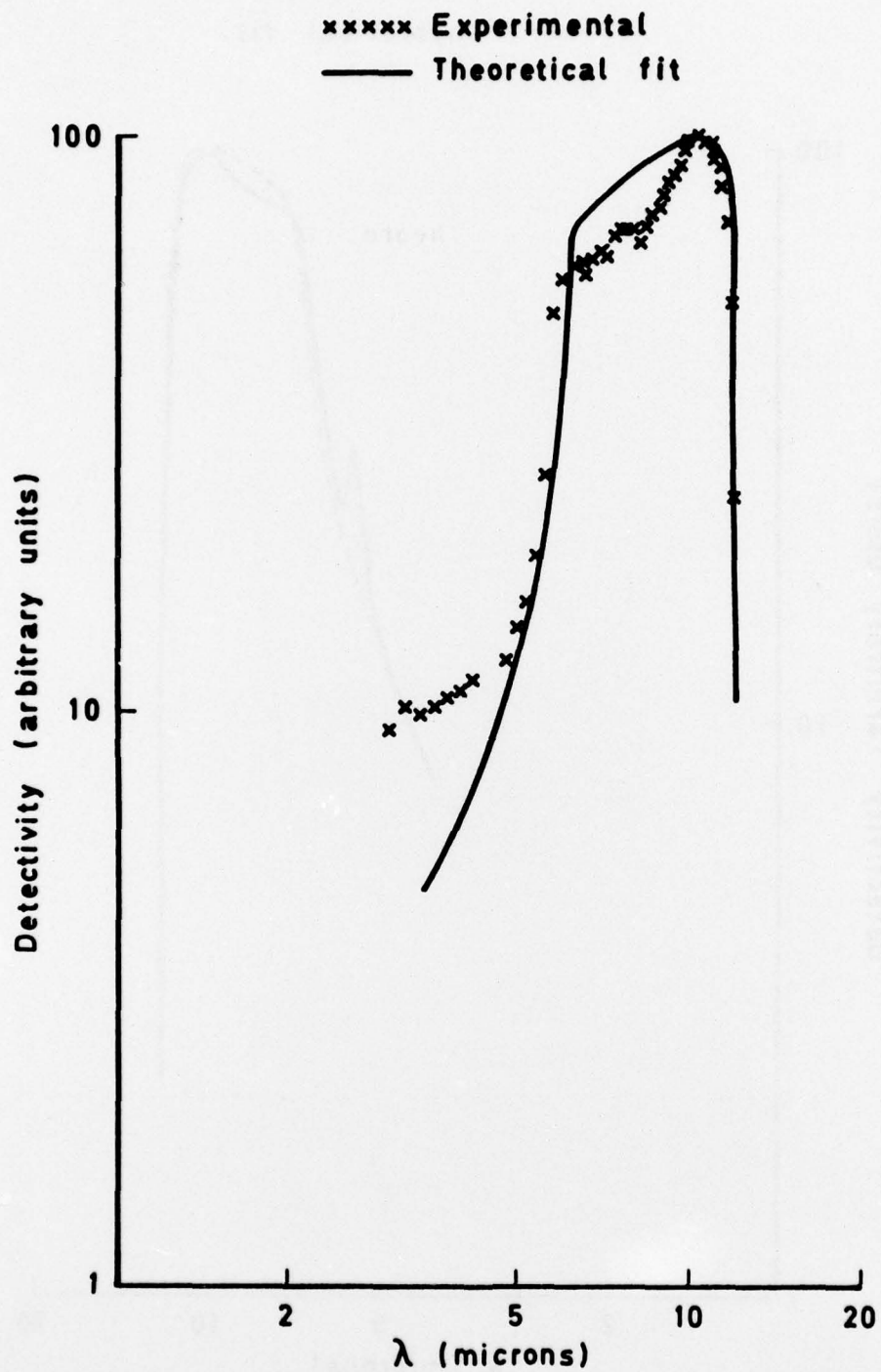


Fig 5 Theoretical fit to response of Santa Barbara heterostructure detector 19-3

Fig 6

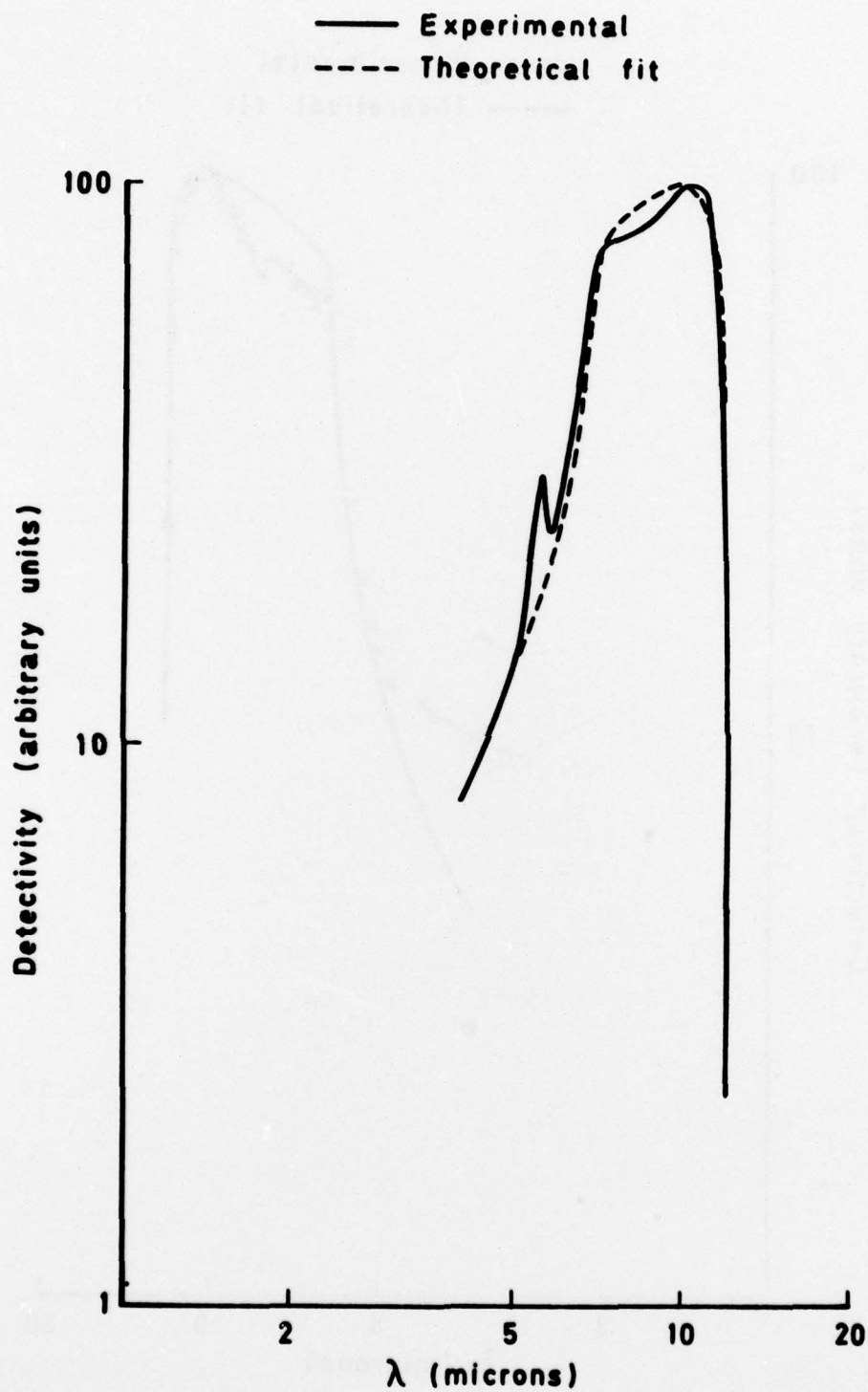


Fig 6 Theoretical fit to response of Plessey heterostructure detector HGF 4/1

Fig 7

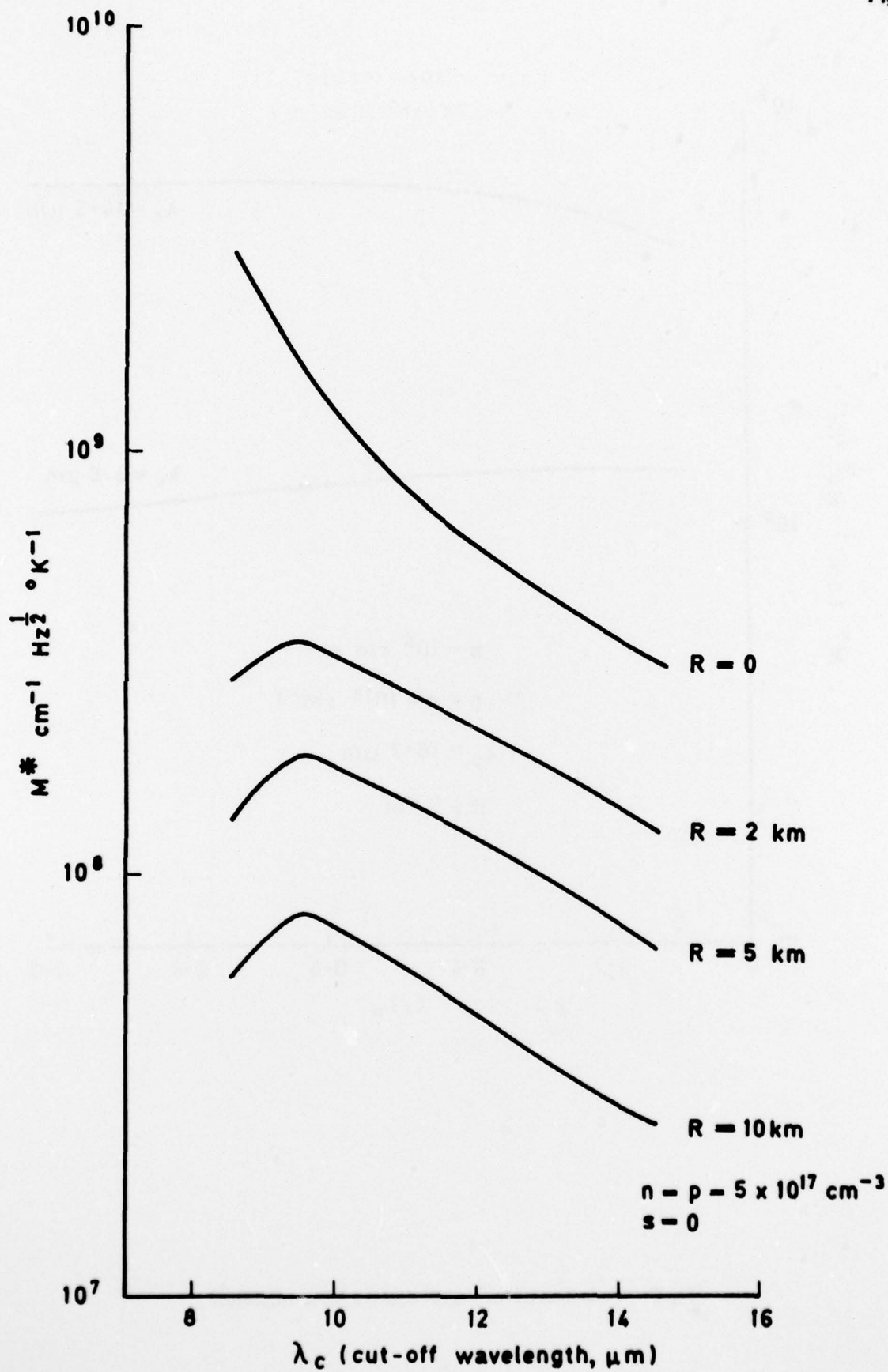
Fig 7 M^* for Pb/SnTe detectors

Fig 8

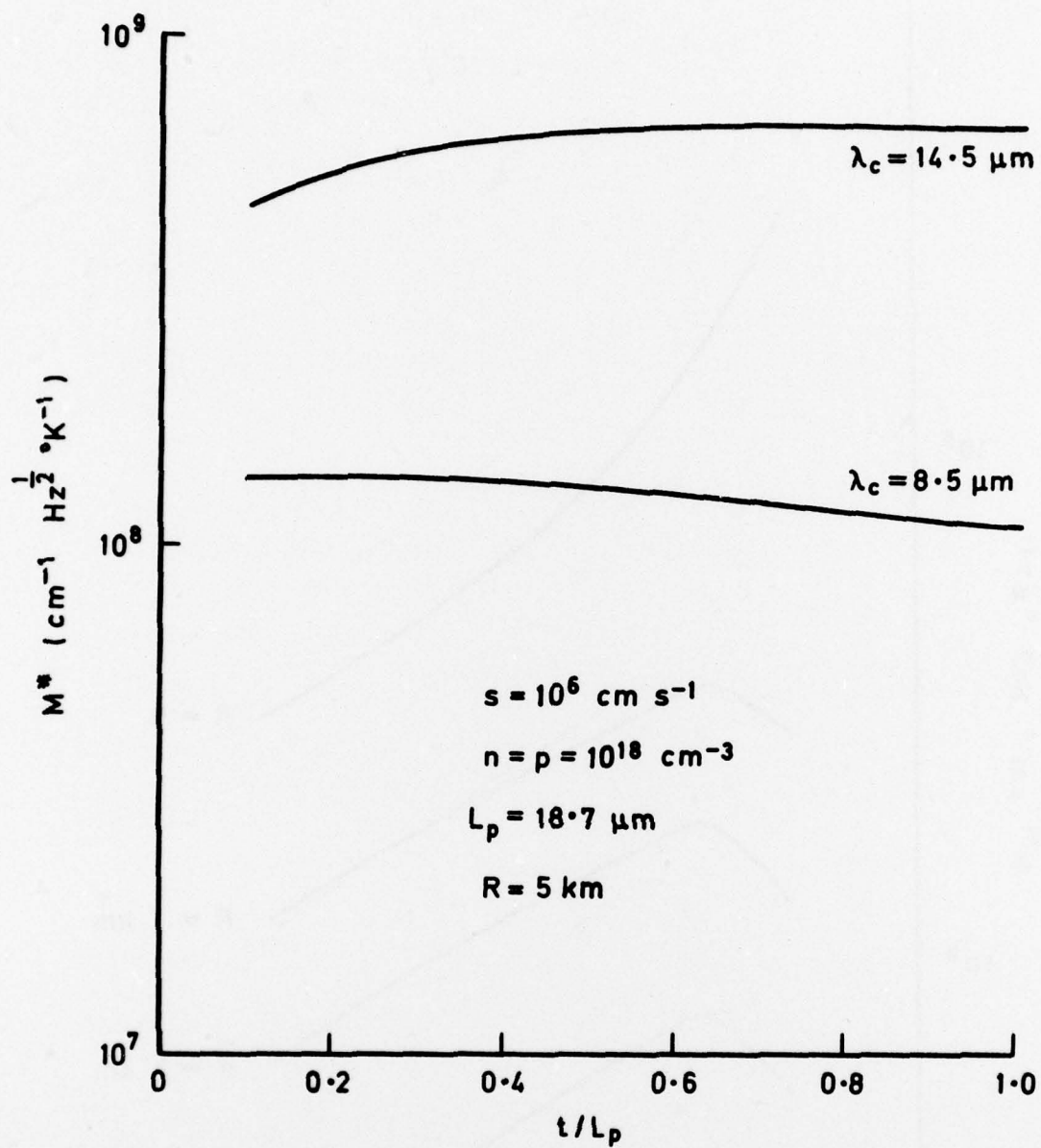


Fig 8 Variation of M^* with surface layer thickness

Fig 9

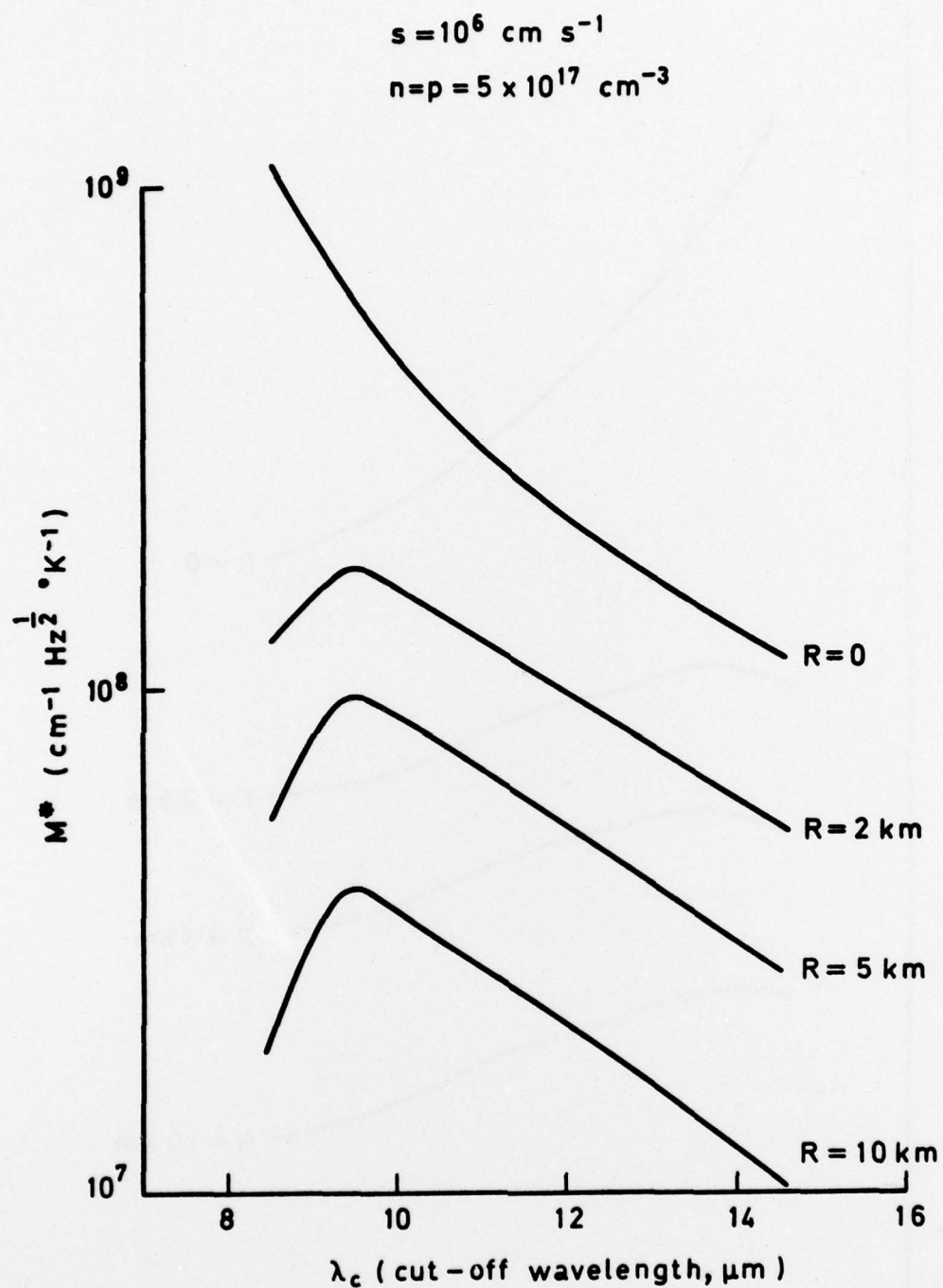


Fig 9 $M^* v$ cut-off wavelength for Pb/SnTe detectors with a high surface recombination velocity

Fig 10

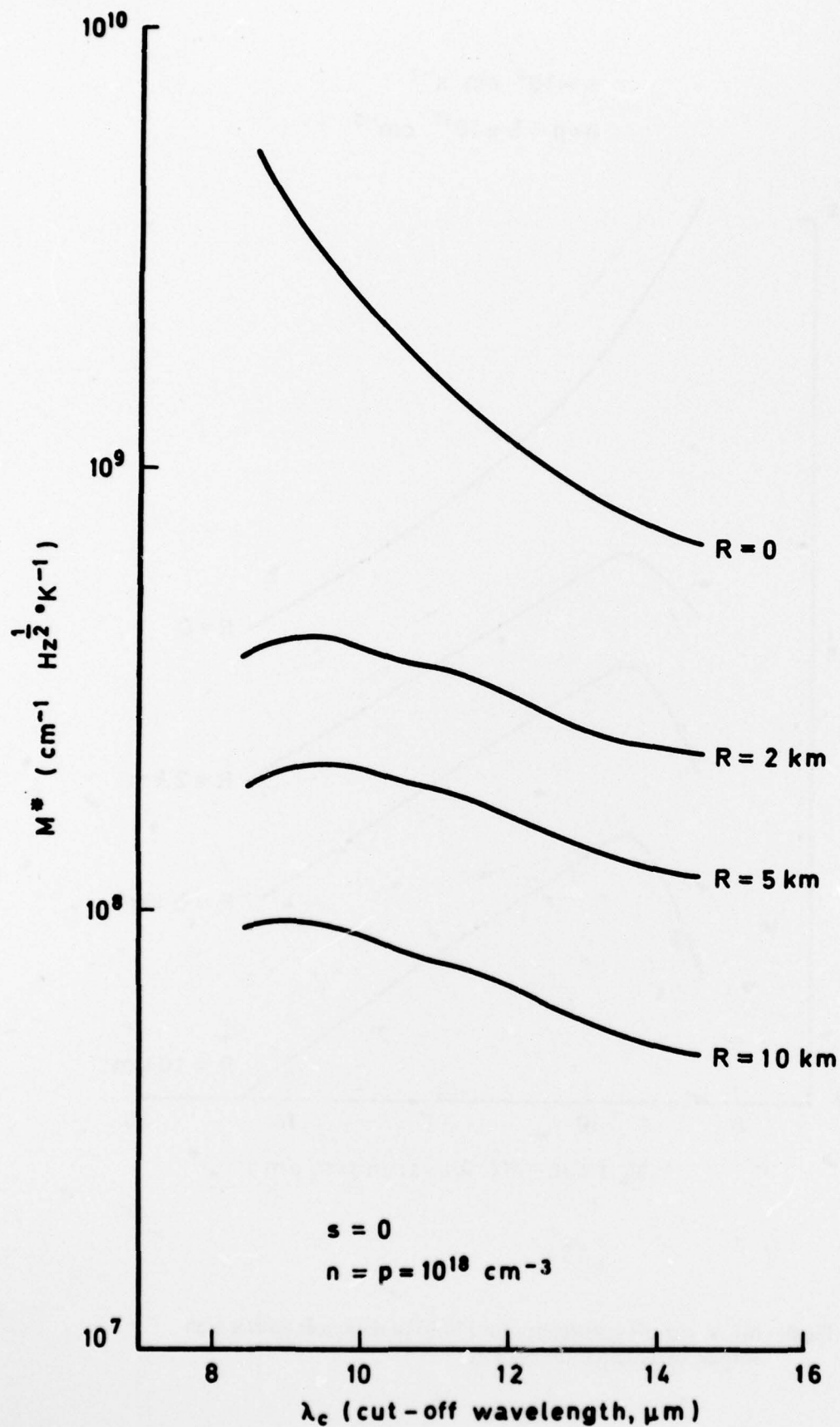


Fig 10 M^* for high carrier concentration detectors

Fig 11

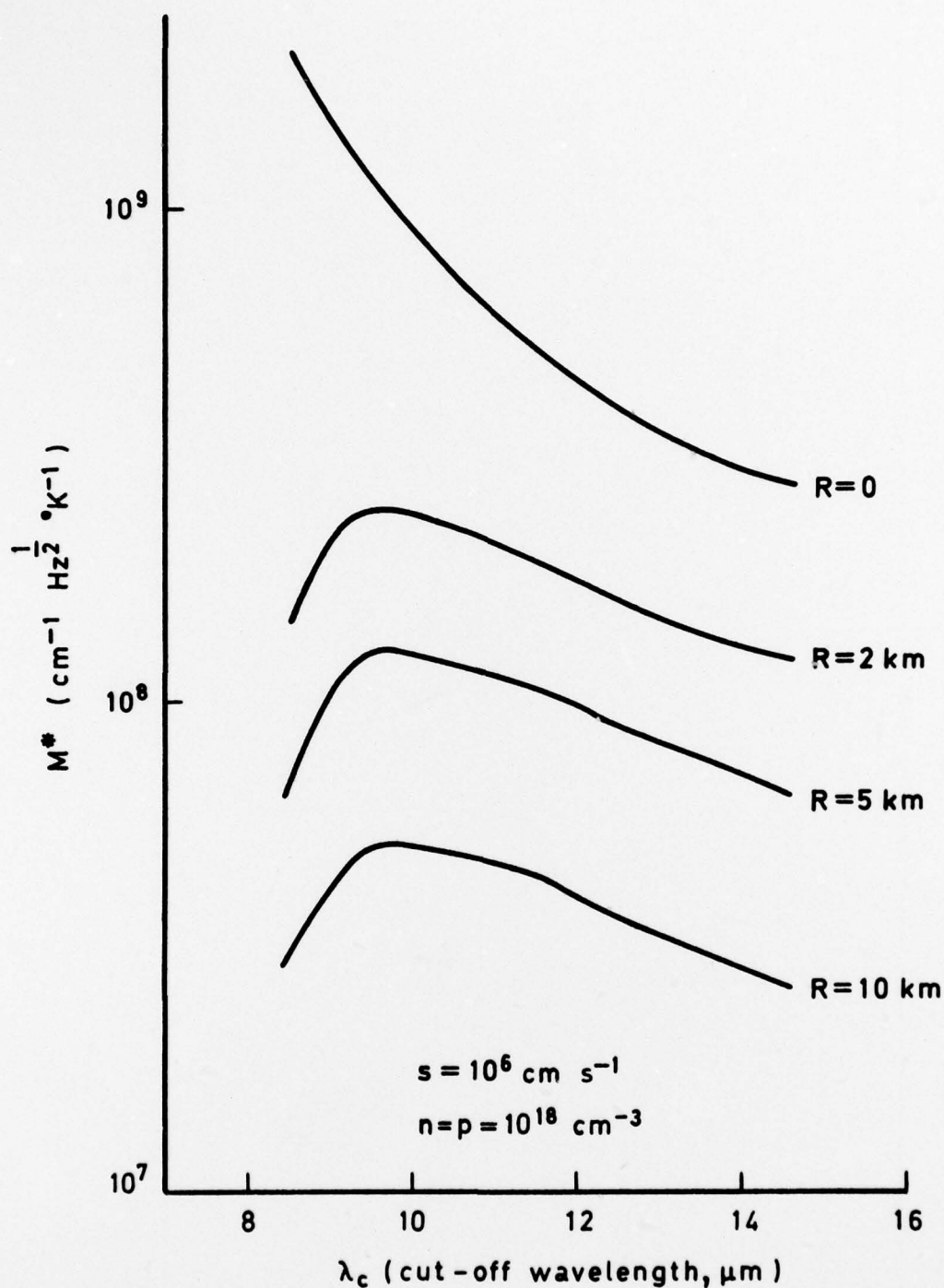



Fig 11 M^* for high carrier concentration detectors with a high surface recombination velocity

REPORT DOCUMENTATION PAGE

Overall security classification of this page

UNCLASSIFIED

As far as possible this page should contain only unclassified information. If it is necessary to enter classified information, the box above must be marked to indicate the classification, e.g. Restricted, Confidential or Secret.

1. DRIC Reference (to be added by DRIC)	2. Originator's Reference RAE TR 77066	3. Agency Reference N/A	4. Report Security Classification/Marking UNCLASSIFIED		
5. DRIC Code for Originator 850100		6. Originator (Corporate Author) Name and Location Royal Aircraft Establishment, Farnborough, Hants, UK			
5a. Sponsoring Agency's Code N/A		6a. Sponsoring Agency (Contract Authority) Name and Location N/A			
7. Title The spectral response of Pb/SnTe detectors					
7a. (For Translations) Title in Foreign Language					
7b. (For Conference Papers) Title, Place and Date of Conference					
8. Author 1. Surname, Initials Ellis, B.	9a. Author 2	9b. Authors 3, 4		10. Date May 1977	Pages 26
11. Contract Number N/A		12. Period N/A		13. Project	
				14. Other Reference Nos. Space 526	
15. Distribution statement (a) Controlled by -  (b) Special limitations (if any) -					
16. Descriptors (Keywords) (Descriptors marked * are selected from TEST) Infra-red detectors. Lead-tin telluride. Burstein-Moss effect. Semiconductor absorption. Atmospheric transmission.					
17. Abstract The effect of the Burstein-Moss shift of the absorption edge on the spectral response of Pb/SnTe detectors is calculated. Calculated spectral responses are compared to published curves for a number of detectors (both homostructure and heterostructure) and some inferences concerning the surface recombination rates and diffusion lengths are drawn. The figure of merit M^* is evaluated for a range of detectors with different cut-off wavelengths.					